Clay Minerals, (2016) **51**, 781–791

Conversion of protonic magadiite to PLS-1 zeolite: thermal stability and acidity

FETHI KOOLI[1,*], JACQUES PLEVERT[2], YAN LIU[3], KAIS HBAIEB[4] AND RAWAN AL-FAZE[1]

[1] *Department of Chemistry, Taibah University, P.O. Box 30002, Al-Madinah Al-Munawwarah, Saudi Arabia*
[2] *Institute of High Performance Computing, 1 Science Park Road #01-01, Singapore 117528*
[3] *Institute of Chemical and Engineering Sciences, 1 Pesek Road, Jurong Island, Singapore 627833*
[4] *Department of Engineering, Taibah University, P.O. Box 443, Al-Madinah Al-Munawwarah, Saudi Arabia*

(*Received 2 March 2016; revised 28 September 2016; Editor: George Christidis*)

ABSTRACT: A synthetic protonic magadiite was used as a silica source to prepare zeolitic material (PLS-1) in the presence of tetramethylammonium hydroxide and water. The conversion of the protonic magadiite to the PLS-1 phase was achieved at 150°C after 5 days, or at 170°C after 3 days for SiO_2:TMAOH:H_2O molar ratios of 2.54:1:4.4. The synthesis of the pure PLS-1 phase depended also on the amounts of tetramethylammonium hydroxide and water used. Analysis by ^{29}Si magic angle spinning nuclear magnetic resonance spectroscopy confirmed the layered character of the PLS-1 phase with a resonance at −93 ppm, and its dehydroxylation-condensation process. The chemical formula of $(TMA)_2Si_{18}O_{33}(OH)_6$ for PLS-1 was refined with the Rietveld method and the tetrahedron-splitting model. The later model has been proposed to describe the presence of silanol defects in the layered structure of PLS-1. Upon calcinations of the PLS-1 phase at temperatures >400°C, the removal of TMA cations and dehydroxlyation of PLS-1 layers resulted in a three-dimensional structure phase identified as the CDS-1 phase, with a chemical formula of $Si_{18}O_{36}$. The CDS-1 phase exhibited a large specific surface area of 288 m^2/g and microporous character, as indicated by the nitrogen adsorption isotherms. The temperature-programmed desorption profile of ammonia indicated that CDS-1 exhibited one weak type of acid sites, confirmed, by pyridine desorption studies, as weak Lewis acid sites.

KEYWORDS: magadiite, layered silicates, PLS-1phase, CDS-1 phase, condensation, acidity.

Most zeolitic materials have been synthesized by conventional methods, involving crystallization of the SiO_2 source in the presence of alkali hydroxides and/or organic bases. The presence of templating or structure-directing agents (SDA) is necessary to form the framework of the zeolite material (Cundy & Cox, 2004, 2005; Burton, 2007; Burton & Zones, 2007). The crystallization takes places in a closed hydrothermal system at increasing temperatures, autogenous pressure and different periods of time (Weitkamp & Puppe, 1999). The type of the SiO_2 source (colloidal solution, precipitated SiO_2, organo-alcoxysilane) has been reported to affect the structural and morphological properties of the zeolites obtained (Bhat & Kumar, 1990; Hamilton *et al.*, 1993; Wiersema & Thompson, 1996; Li *et al.*, 2000; Karami & Rohani, 2009). It affects the types of zeolites synthesized (Warzywoda *et al.*, 1995), the crystal size (Warzywoda *et al.*, 1996; Kalipcilar & Culfaz, 2001; Li *et al.*, 2001), the morphology (Hamidi *et al.*, 2003) and the rate of crystallization (Antoni *et al.*, 1999).

Zeolites prepared from different sources of natural clay minerals are always contaminated with trace amounts of Fe, Ti, Ca, Mg, *etc*. present in the original raw materials. These elements might influence the zeolite properties (Ruiz *et al.*, 1997; Cañizares *et al.*, 2000;

* E-mail: fkooli@taibahu.edu.sa
https://doi.org/10.1180/claymin.2016.051.5.07

Boukadir *et al.*, 2002; Lee *et al.*, 2003; Mignoni *et al.,* 2009; Ríos *et al.*, 2009). The use of synthetic layered silicates was proposed as an alternative source of SiO_2 due to the purity of the crystalline products. Synthetic layered silicates have been used for the synthesis of pure SiO_2, zeolites and mesoporous materials (Pál-Borbély *et al.*, 1997; Selvam *et al.*, 2003, 2014; Ikeda *et al.*, 2009; Wang *et al.*, 2010a,b; Dhainaut *et al.*, 2013; Moura & Pastore, 2014) and especially, Na-magadiite (Na-mag, Wang *et al.*, 2010a,b; Cui *et al.*, 2014; Kooli *et al.,* 2002a,b). The latter has received significant attention because of its ability to transform to layered silicic acid by proton exchange in acidic solution (Lagaly *et al.*, 1975). Moreover, it is a useful host in the formation of pillared materials due to the presence of reactive silanol groups in their interlayer surface (Park *et al*., 2009; Kim *et al.*, 2012).

The tetramethylammonium hydroxide (TMAOH) is considered to be the simplest structure-directing agent (SDA) for the synthesis of a variety of zeolite structures. It has been used either alone or together with other SDAs to prepare new zeolite phases (Oberhagemann *et al.*, 1996; Pinar *et al.*, 2007; Asakura *et al.*, 2014; Benabdallah Benarmas *et al.,* 2014; Marler *et al.*, 2014; Xue *et al.*, 2015; Yin *et al.*, 2015). Indeed, the recrystallization of Na-mag in the presence of pure TMAOH solution yielded PLS-1 phase at temperatures <150°C after 3 days (Kooli *et al.*, 2001a). The structure of the PLS-1 (Pentagonal Cylinder Layered Silicate-1) precursor consists of silicate that adopts shared faces of pentagonal cylinders made up of five-membered silicon, or pentasil, rings (Ikeda *et al.*, 2004). Using protonic magadiite (H-mag) where Na^+ cations were exchanged with protons in HCl solution, the conversion occurred at 150°C after 5 days, using the same SDA (Kooli *et al.*, 2001b). The PLS-1 precursor exhibited greater thermal stability and was transformed to another CDS-1 (Cylindrically Double Saw Edge Zeolite) phase after calcination at 400°C and above, due to the topotactic dehydration-condensation between the silicate layers of PLS-1. The magadiites used in previous studies (Kooli *et al.*, 2001a,b) were provided by the Clariant company (Japan), and used as received without prior knowledge of their synthesis conditions. In the present study, the authors were interested in understanding how the origin of Na-magadiite could affect its reaction with TMAOH solution. For this purpose, Na-magadiite and its protonic derivative were prepared fresh in the laboratory, following the method used in previous studies. The effect of different factors such as temperature of hydrothermal treatment, period of treatment, and the TMAOH and water contents were investigated. In previous studies, the addition of dioxane as a solvent reduced the duration of synthesis of some zeolites from 3 days to a matter of hours and affected the nucleation and rearrangement of the soluble SiO_2 species around the TMA cations (Kooli *et al.*, 2001a; Kawai *et al.*, 2010). The effect of dioxane on the conversion of H-mag was also investigated. The characterization of the precursors and the calcined products were performed using various techniques. The variation of textural properties upon calcination of the resulting material (PLS-1) was examined by nitrogen adsorption isotherms. The tetrahedron-splitting model was proposed in the Rietveld refinement to correlate the theoretical and experimental chemical formulae of the PLS-1 phase. For the first time, the thermal stability of PLS-1 was investigated using an *in situ* Raman technique, and the acidity of the resulting CDS-1 zeolite was investigated using temperature-programmed desorption (TPD) of ammonia and pyridine as probe molecules.

EXPERIMENTAL

Materials

The chemicals used were of analytical reagent grade: Ludox HS-40 (colloidal SiO_2), solid NaOH and TMAOH solution (25% in water) were purchased from Aldrich (Germany) and used as received.

Synthesis of Na-mag and derivatives

Na-mag was prepared by the reaction of a SiO_2-NaOH-H_2O system under hydrothermal conditions (Kooli & Yan, 2009). 4.8 g of NaOH was dissolved into 105 mL of deionized water and 45 g of colloidal SiO_2 was added dropwise to the NaOH solution over 30 min to form a gel with molar composition Na_2O:5SiO_2:122H_2O. The gel was stirred for 1 h at room temperature, then it was transferred to a Teflon®-lined autoclave and heated under autogeneous pressure at 150°C for 2 days.

H-mag was prepared by ion exchange of Na-mag (2 g) in HCl solution (200 mL, 0.1 N) for 2 h at room temperature. The solid was filtered, washed with deionized water until the chloride test with $AgNO_3$ solution was negative, and then air-dried at room temperature. The sample was ground with an agate mortar and kept in glass vial in a desiccator.

Synthesis of PLS-1 materials

1 g of H-mag was added to 2.25 mL of TMAOH (25% in mass) and 0.5 mL of water, corresponding to a

https://doi.org/10.1180/claymin.2016.051.5.07 Published online by Cambridge University Press

molar ratio of SiO_2:TMAOH:H_2O = 2.5:1:4.4. The water amount given took into account the water content in the TMAOH solution. The reaction mixture was heated under autogenous pressure in a Teflon-lined autoclave at 150°C for 5 days. The resulting product was filtered, washed with water and dried at room temperature overnight. The sample was ground with an agate mortar and kept in a desiccator.

The parameters affecting the conversion of H-mag were investigated individually, by varying only one parameter, and keeping the others constant. The amount of TMAOH aqueous solution varied from 1.0 to 4.5 mL, and the amount of water added, between 0.25 and 2 mL. The temperature varied from 150°C to 170°C, and reaction time from 3 to 7 days was used. Table 1 summarizes the different parameters investigated in the present study.

In one case, an additional 5 mL of dioxane was added to a mixture of H-mag, TMAOH and water (sample 8). The mixture was treated in a closed, Teflon-lined autoclave at 150°C for 7 days. The resulting solid was filtered, washed with excess water and dried at room temperature overnight.

The precursor PLS-1 phase was calcined under air atmosphere, in the temperature range of 300–1000°C for 4 h at a heating rate of 5°C min^{-1}, to burn out the SDA molecules. The sample name PLS-1(300) indicates that the PLS-1 precursor was calcined at 300°C, *etc*.

Characterization techniques

Powder X-ray diffraction (XRD) patterns were obtained using a Bruker D8 Advance diffractometer equipped with Ni-filtered Cu-*K*α radiation. The patterns were recorded in the range of 1.5–50°2θ with a scan speed of 1°2θ/min and a scan step size of 0.02°. Thermogravimetric analysis (TGA) was carried out on a TA Instruments SDT2960 analyser, with an air flow of 100 mL min^{-1} on samples heated from 25 to 800°C, at a heating rate of 5°C min^{-1}. The BET specific surface area, pore volume at p/p_o of 0.97, *t-plot* method for the micropore surface area, and pore-size distributions were estimated by N_2 adsoprtion isotherms, using a Quantachrome Autosorb A6 instrument. The samples were degassed at 300°C overnight prior to the measurements. ^{29}Si magic angle spinning (MAS) nuclear magnetic resonance (NMR) spectroscopy was performed using a Bruker 400 spectrometer, operating at a ^{29}Si NMR frequency of 78 MHz. A 4-mm MAS probe was used with sample-rotation rates of 8.0 kHz. 80–100 scans were accumulated with the recycle delay from 200 to 400 s. The area ratio of the different resonances was estimated by fitting operation using the *Grams* program. The ^{1}H-^{29}Si cross-polarization (CP)/MAS spectra were recorded with a standard CP sequence at a spinning speed of 8 kHz. The recycle delay between consecutive scans was 10 s. The chemical shifts are reported with respect to tetramethylsilane (TMS). ^{1}H-^{13}C CP solid-state (^{13}C CP MAS) NMR spectra were acquired using a Bruker Advance DSX400 spectrometer operating at 400.16 MHz for ^{1}H and 100.56 MHz for ^{13}C with a MAS triple resonance probehead using zirconia rotors 4 mm in diameter. The spinning rate was 4.0 kHz, the ^{1}H π/2 pulse length was 4.40 μs, the contact time was 1.0 ms and the pulse delay was 10.0 s. The *in situ* Raman studies were recorded using a Linkam cell, by heating the sample at 50°C, 100°C, 250°C, 300°C, 400°C and 425°C, respectively, with a heating rate of 5°C/min, under air atmosphere. A Renishaw Raman

Table 1. Compositions of the reagents (molar ratios) and the reaction products.

Samples	SiO_2	TMAOH	H_2O	Temp., duration	Phases
Sample 1	2.54	1	4.4	150°C, 5 days	PLS-1
Sample 2	2.54	1	4.4	170°C, 3 days	PLS-1
Sample 3	2.54	0.43	4.4	150°C, 5 days	TMA-mag and PLS-1
Sample 4	2.54	1.90	4.4	150°C, 5 days	Amorphous silica
Sample 5	2.54	1	2.2	150°C, 5 days	PLS-1
Sample 6	2.54	1	6.6	150°C, 5 days	PLS-1 and TMA-mag
Sample 7	2.54	1	16.6	150°C, 5 days	Amorphous silica
Sample 8*	2.54	1	4.4	150°C, 7 days	TMA-mag

TMA-mag: tetramethylammonium-intercalated magadiite.
*Adding 5 mL of dioxane.

https://doi.org/10.1180/claymin.2016.051.5.07 Published online by Cambridge University Press

microscope was used to record the Raman spectra at the real heating temperature values without cooling the sample.

For structural refinement, the powder XRD patterns were collected using a Bruker D5005 X-ray diffractometer operating in Bragg-Brentano geometry, equipped with a graphite monochomator and Soller slits using Cu-$K\alpha$ radiation. The powder XRD patterns were indexed using the program *TREOR* (Werner *et al.*, 1985). The *GSAS* software package was used for the Rietveld refinement and the Fourier analysis of the structures.

The acidity of PLS-1(500) was investigated using ammonia temperature-programmed desorption, and pyridine desorption at different temperatures under vacuum, following the same procedures as reported in previous studies (Kooli *et al.*, 2008, 2016a).

RESULTS AND DISCUSSION

Na-mag and PLS-1 materials

The Na-mag was obtained as a single phase after a reaction periods of 2 days. The powder XRD patterns of the product matched well those of Na-magadiite reported in the literature (Li *et al.*, 2005; Kooli & Yan, 2009; Park *et al.*, 2009) (Fig. 1). The basal spacing was ~1.54 nm, with reflections, indicating the well ordered structure of the synthesized Na-mag (Ogawa *et al.*, 2002). The acid treatment of Na-mag with HCl solution induced peak broadening due to a decrease in the degree of crystal order and shrinkage of the basal spacing from 1.54 to 1.21 nm, associated with the exchange of Na^+ cations with protons (Li *et al.*, 2005; Kooli & Yan, 2009). The conversion of H-mag to a silicate phase was achieved at 150°C after 5 days, and at 170°C after 3 days. The powder XRD pattern of this silicate phase coincided well with the PLS-1 phase with a major reflection at 1.09 nm (Fig. 1). On the other hand a mixture of PLS-1 and intercalated TMA-magadiite was obtained after 3 days at 150°C (Fig. 1). These results were different from those reported in a previous study using a different H-mag (Kooli *et al.*, 2001a). This difference could be related to the origin of the starting SiO_2 source.

The conversion of H-mag to a pure PLS-1 phase was related to the amount of TMAOH solution used at 150°C for 5 days. When of 0.5 mL of TMAOH solution was added, only intercalated TMA-magadiite was obtained with a basal spacing of 1.91 nm (sample 3). For 1 g of H-mag, conversion to the PLS-1 phase was achieved (sample 1). For greater amounts of TMAOH solution

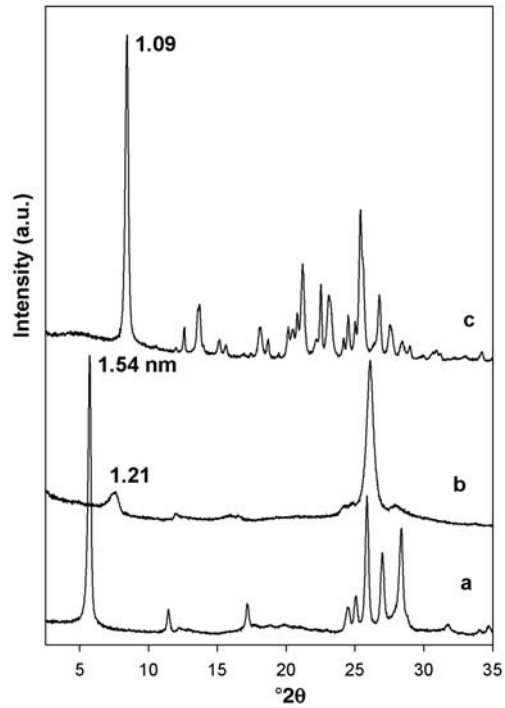

FIG. 1. Powder XRD patterns of: (a) Na-magadiite; (b) H-magadiite; and (c) after conversion to the PLS-1 phase at 150°C for 5 days.

(~3 mL, sample 4), conversion of H-mag to amorphous SiO_2 was observed (Table 1).

Four experiments were performed by fixing the amount of TMAOH and H-mag, and using various amounts of water (samples 1, 5, 6, 7). The conversion of H-mag to PLS-1 was achieved for added amounts of TMAOH ≤0.5 mL (sample 1, 5) whereas for amounts of water added of 1 mL (sample 6), a mixture of PLS-1 and TMA intercalated phases was obtained (Table 1). However, H-mag was converted to an amorphous phase for water contents of 2 mL in the mixture (Table 1).

Although dioxane was expected to shorten the reaction time, the addition of dioxane to a mixture of H-mag, TMAOH and H_2O, (sample 8), did not activate its conversion even after 7 days at 150°C, and intercalated TMA-mag was obtained with a phase having a diffraction maximum of 1.91 nm.

Figure 2 presents the powder XRD patterns of the PLS-1 phase calcined up to 1000°C, in air atmosphere. At 300°C, the PLS-1 phase was transformed to two different phases, with diffraction maxima at 0.98 and 0.92 nm. These phases could be related to a transition

https://doi.org/10.1180/claymin.2016.051.5.07 Published online by Cambridge University Press

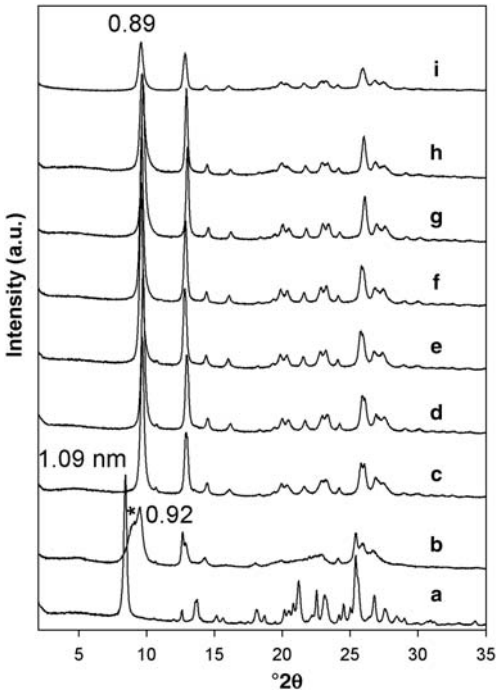

FIG. 2. Powder XRD patterns of the original PLS-1 phase (a), and after calcination at: (b) 300°C, (c) 400°C, (d) 500°C, (e) 600°C, (f) 700°C, (g) 800°C, (h) 900°C and (i) 1000°C. * corresponds to the phase at 0.92 nm.

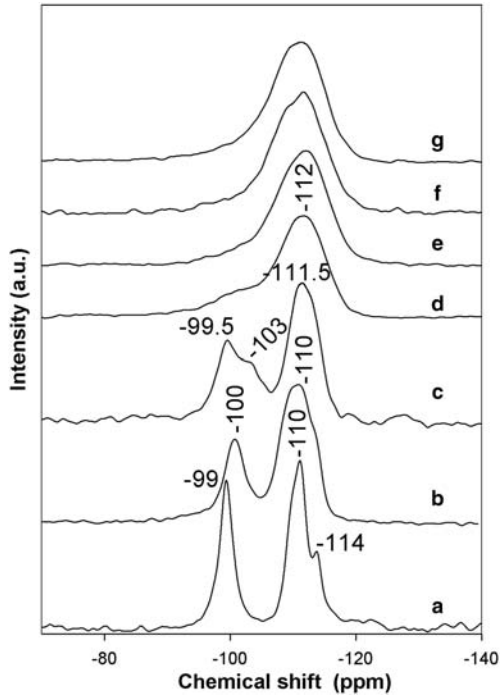

FIG. 3. Solid ^{29}Si MAS NMR of: (a) Na-magadiite; (b) H-magadiite; and (c) FLS1 phases treated at: (d) 300°C, (e) 500°C, (f) 700°C and (g) 900°C.

phase prior to the complete oxidation of TMA cations which occurred at 386°C (deduced from a TGA study, Kooli *et al.,* 2016b). After heating at 400°C, the main diffraction maximum of PLS-1 shifted from 1.09 to 0.89 nm, due to the dehydration-condensation of the silicate layers (Kooli *et al.*, 2001b; Ikeda *et al.*, 2004; Solânea *et al.*, 2013). A similar phase was obtained after calcination at 800°C. The intensity of the powder XRD reflections decreased dramatically at 1000°C due to poor crystal order of PLS-1(1000). The XRD patterns of the calcined PLS-1 precursor at temperatures ≥400°C coincided well with the CDS-1 material with some variation of the peak intensity (Fig. 2).

The intercalation of TMA cations occurred at an early stage of the conversion of H-mag, and similar data were obtained also from starting Na-mag (Table 1). As the amount of TMAOH increased, or the amount of water decreased to a certain ratio, the conversion of TMA-magadiite to PLS-1 occurred progressively and was completed either at 3 days or 5 days, depending on the reaction temperature. Further increase of TMAOH/water ratios led to partial conversion.

Solid NMR studies

The ^{29}Si MAS NMR spectra of pure Na-mag exhibited two well separated resonances corresponding to two Si environments: one Q^3 type where Si was bound to three [SiO_4] tetrahedra and one OH group, centred at −99 ppm, and one Q^4 Si type with a broad resonance at −110 to −114 ppm (Eypert-Blaison *et al.*, 2001; Bi *et al.*, 2012) (Fig. 3). During acid treatment, the layered structure was maintained and a similar spectrum obtained (Eypert-Blaison *et al.*, 2001). After reaction with TMAOH solution, the PLS-1 sample exhibited two single resonances at –99.5 and –111.5 ppm, attributed to different Si types, in good agreement with previous data (Kooli *et al.*, 2001a; Ikeda *et al.*, 2004). The resonance at −99.5 pm was related to Q^3 species ($HOSi(OSi)_3$) and that at −111.5 ppm was assigned to Q^4 species ($Si(OSi)_4$). The shoulder at −103 ppm could be assigned to different Q^3 species. After calcination at 300°C, the resonance of the Q^3 species decreased and disappeared completely at temperatures in excess of 400°C due to dehydroxylation and condensation of the silicate layers. At higher temperatures the spectra exhibited a

https://doi.org/10.1180/claymin.2016.051.5.07 Published online by Cambridge University Press

broad resonance centred at −112 ppm, assigned mainly to the Q^4 species (Kooli *et al.*, 2001b; Ikeda *et al.*, 2004).

More information about the assignment of ^{29}Si CP/MAS NMR lines can be obtained using ^{1}H-^{29}Si CP/MAS measurements (Gontier & Tuel, 1996; Günter, 2007). The CP/MAS NMR spectra for the original and the calcined PLS-1 phase at 300°C are presented in Fig. 4. The Q^3 resonance at −101 ppm was enhanced, compared to the ^{29}Si signal, confirming the presence of silanol groups for the original PLS-1. These Q^3 groups are associated with the silicate layers. The low abundance of the Q^3 environments in the CP spectra of the PLS-1 calcined at 300°C indicates that calcination resulted in the dehydroxylation of the silicate layer, and its condensation to form a three dimensional network, with increase of the resonance of the Q^4 species, in good agreement with the powder XRD data. As the calcination became enhanced, this resonance disappeared completely, and a new, additional resonance appeared at –105 ppm. The intensity of the latter also decreased continuously at 700°C (Fig. 4).

The ^{13}C solid state NMR of the PLS-1 confirmed the presence of TMA cations in its structure with a single, quite sharp resonance at 58 ppm (Kooli *et al.,* 2016b). This value is comparable to that reported for TMA cations in other zeolite structures (Den Ouden *et al.*, 1991; Marler *et al.*, 2014). The narrow line may indicate that there was some mobility of the TMA in its environment (Fan *et al.*, 2006). However, for the CDS-1 material, the spectrum did not exhibit a resonance at 58 ppm, which confirmed that the material was free of TMA cations.

In situ spectroscopy studies

The *in situ* Raman microscope spectrum of the as-prepared PLS-1 material is presented in Fig. 5. The spectrum exhibited sharp characteristic bands due to the symmetric and asymmetric C–N stretching vibration modes of TMA at 750 and 947 cm^{-1}, respectively (Suk-Bong, 1995). The CH_3 deformation vibration was detected at 1453 cm^{-1}. Because of the shift in the frequencies of TMA upon encapsulation (especially

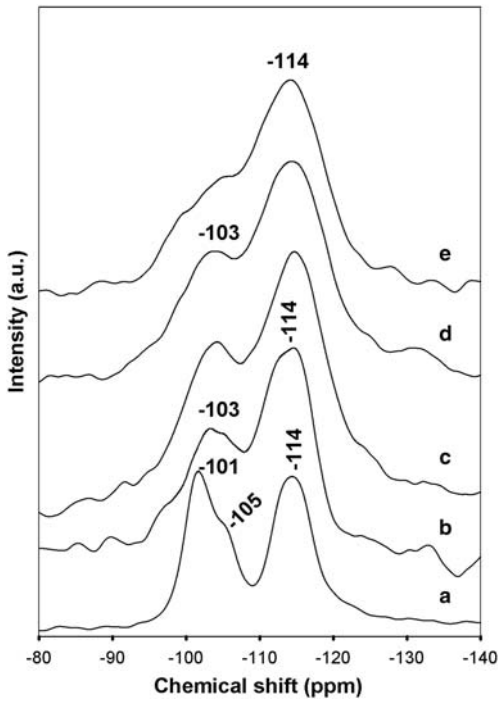

FIG. 4. Solid-state ^{1}H-^{29}Si CP/MAS NMR (a) of the PLS-1 phase and the PLS-1 treated at different temperatures, (b) 300°C, (c) 400°C, (d) 600°C and (e) 700°C.

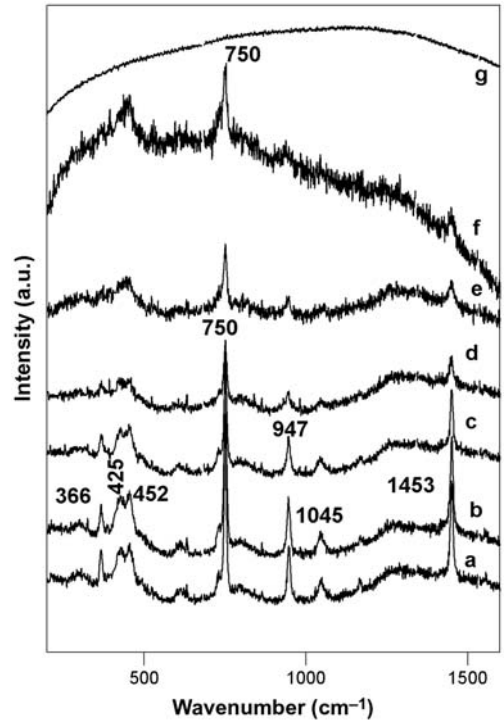

FIG. 5. *In situ* Raman spectra of the PLS-1 phase treated at: (a) room temperature, (b) 50°C, (c) 100°C, (d) 250°C, (e) 300°C, (f) 400°C and (e) 425°C.

https://doi.org/10.1180/claymin.2016.051.5.07 Published online by Cambridge University Press

the C–N stretching mode from 754 to 766 cm^{-1}), it is relatively easy to distinguish between free and bound TMA cations (Dutta *et al.,* 1986; Hong, 1995). The recorded values are close to those reported for TMA cations in D_2O solutions (Hong, 1995; Ouasri *et al.,* 2002), and indicated that the TMA cations in PLS-1 material were located between the silicate layers and moved easily in the interlayer space of layered silicate. Upon heating at 200°C, the intensity of these bands decreased gradually until they disappeared completely at temperatures of >400°C (Fig. 5). The temperature was in good agreement with the TGA studies. Surprisingly, the specific bands related to Si–O bands in the range 1200 to –1000 cm^{-1} were not detected in the present study. Similar results were noted when studying the thermal stability of organo-magadiites (Kooli & Yan, 2009).

Textural and morphological properties

The isotherms of PLS-1 were of type II, typical of non-porous materials, while the calcined PLS-1 materials exhibited type I isotherms in the low relative pressure range, due to the microporous character of these materials (Gregg & Sing, 1982). The microtextural properties of the samples are summarized in Table 2. The starting PLS-1 containing TMA molecules exhibited a small specific surface area (32 m^2 g^{-1}) and micropore volume of 0.0063 cc g^{-1}. After the elimination of TMA molecules, the specific surface area increased gradually to 265 m^2 g^{-1} with a pore volume of 0.16 cc g^{-1} at 600°C. The greater specific-surface-area and pore-volume values were maintained up to 800°C with a slight decrease. At 1000°C, a reduction of these properties was observed due to the collapse of the three-dimensional structure. The contribution of the micropore surface area to the total surface area was in the range of 62–69% for samples calcined at temperatures >300°C. At lower temperatures, the contribution was only ~10%, indicating that the access of nitrogen molecules was blocked by the TMA cations. The average pore-size values were 2.8–3 nm. The values recorded were smaller than those of CDS materials that were obtained from different magadiite sources, and were calcined at the same temperatures for different heating rates and periods (Kooli *et al.*, 2002)

The SEM images indicated that magadiite materials have lost their initial morphology (not shown), and the PLS-1 materials exhibited a platy morphology, with different size and agglomeration, depending on the calcination temperature.

Proposed chemical formulae

In spite of recent advances, the crystal-structure solution of complex zeolites from powder XRD data still remains a challenge. One way to improve the phase refinement is to take advantage of the characteristics specific to the zeolites (Brenner *et al.*, 2002). The refinement conditions for the as-synthesized (PLS-1) phase were based on the model reported by Ikeda *et al.* (2004). The chemical formula of the layered phase calculated from the contents of the unit cell was $(TMA)_2Si_{18}O_{34}(OH)_4$. The estimated ratio $Q^3/Q^4 = 0.286$ was much lower than the experimental ratio $Q^3/Q^4 = 0.5$ obtained from ^{29}Si MAS NMR data. The

TABLE 2. Microtextural properties of the FLS1 phase calcined at different temperatures.

Samples	SSA (m^2g^{-1})	M.S.A (m^2g^{-1})	T.P.V. (cc/g)	A.P.S (nm)
PLS-1	32.10	3.50	0.063	7.81
300°C*	68.21	7.01	0.205	12.0
400°C	230.21	160.02	0.164	2.85
500°C	253.81	163.21	0.294	2.64
600°C	288.12	180.24	0.212	2.95
700°C	265.01	174.21	0.203	3.06
800°C	256.5	163.90	0.193	3.02
900°C	126.41	79.10	0.093	2.95
1000°C	65.02	0.02	0.102	9.81

300°C* indicates that PLS-1 was calcined at 300°C. M.S.A.: micropore surface area. T.P.V.: total pore volume. A.P.S.: average pore size.

https://doi.org/10.1180/claymin.2016.051.5.07 Published online by Cambridge University Press

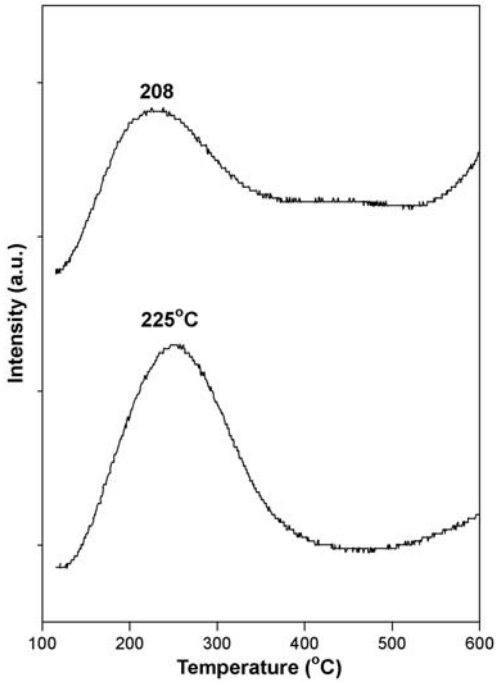

FIG. 6. Temperature-programmed desorption (TPD) of ammonia curves adsorbed on PLS-1 samples calcined at (a) 500°C, (b) 700°C.

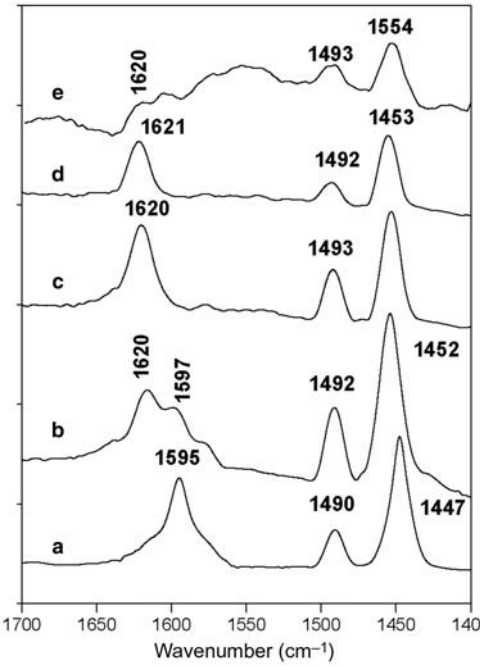

FIG. 7. FTIR spectra of pyridine (a) adsorbed on PLS-1 calcined at 500°C, and desorbed at: (b) room temperature, (c) 100°C, (d) 200°C and (e) 300°C.

layered structure is probably defective and additional silanol groups are present within the structure. A simple tetrahedron-inversion model was introduced to improve the refinement, and the chemical formula of the defective structure was $(TMA)_2Si_{18}O_{33}(OH)_6$. The additional OH groups increased the ratio $Q^3/Q^4 = 0.50$, close to the experimental value. The shoulder on the Q^3 peak in the ^{29}Si MAS NMR spectrum confirmed the presence of the additional silanol groups in the structure.

The powder XRD pattern of the as-synthesized phase showed a shift of the strong first diffraction line from 8.5 to 9.6°2θ after thermal treatment at 400°C as described above (Fig. 2). The line presents some asymmetry on the high-angle side, indicating that the calcined phase consists of layers that condense upon calcination to form a three-dimensional structure. The asymmetry of the basal line indicated that the condensation of the layers was not perfect and that some stacking faults or turbostratic disorder occur. The refined structure of calcined PLS-1(500) was based also on the model reported for CDS-1(Ikeda *et al.*, 2004) and the chemical formula was estimated as $Si_{18}O_{36}$ from the unit-cell contents.

Characterization of acidity

The TPD of ammonia was used to study whether strong or weak acidic sites, or both, are present on the CDS-1 surface (Bagnasco, 1996). The NH_3-TPD profiles of PLS-1 calcined at 500°C and 700°C, are presented in Fig. 6. The maximum desorption peaks of ammonia occurred at 225°C and 208°C, respectively. Qualitatively, a smaller amount of NH_3 was desorbed from PLS-1 calcined at 700°C than at 500°C, and the temperature of the maximum of the desorption peaks shifted gradually to smaller values with increasing calcination temperature of the PLS-1 precursor. The desorption curve shows significant tailing but overall seems to be a single desorption process as there are no visible shoulders in the curve. The temperature values demonstrate weak adsorption sites for ammonia.

The acidic sites could not be identified as either Brönsted- or Lewis-type sites, using TPD ammonia (Kresnawahjuesa *et al.*, 2002; Niwa & Katada, 2013). For this reason, desorption of the pyridine molecule at different temperatures under vacuum was used to identify the nature of the acid sites and their strength. The FTIR spectra of pyridine (pyr) adsorbed and

https://doi.org/10.1180/claymin.2016.051.5.07 Published online by Cambridge University Press

desorbed at room temperature on PLS-1(500) and outgassed at different temperatures, are presented at Fig. 7. The spectrum exhibits an intense band at 1595 cm^{-1}, similar to that recorded after adsorption of pyr on SiO_2 (Kondo *et al.*, 2010), which was assigned to pyr hydrogen-bonded to Si-OH groups. After outgassing at room temperature, this band decreased dramatically in intensity, and a new one was recorded at 1620 cm^{-1}, together with additional bands at 1491 and 1452 cm^{-1}, which were ascribed to modes 8a, 19a and 19b of pyr adsorbed on surface Lewis-acid sites (Khabtou *et al.*, 1994; Buzzoni *et al.*, 1996). These bands were recorded after thermal treatment at 100°C and 200°C, with a decrease in intensity, and were observed as traces after treatment at 300°C (Fig. 7). These data indicate that the PLS-1(500) exhibited some weak Lewis acid sites.

Similar observations were recorded for the PLS-1 calcined at temperatures >500°C. The FTIR data indicated that the Lewis sites became weaker as calcination temperatures of PLS-1 increased, and the pyr molecules were desorbed completely under vacuum at 100°C for PLS-1 calcined at 1000°C.

CONCLUSIONS

H-magadiite was prepared in the laboratory; it was reacted with TMAOH solution and water, under autogenous pressure. The PLS-1 phase was obtained at 150°C after 5 days, and at 170°C after 3 days, with a refined chemical formulae of $(TMA)_2Si_{18}O_{33}(OH)_6$, determined from the unit cell. The CDS-1 phase (with chemical formula of $Si_{18}O_{36}$) was obtained after calcination of the PLS-1 phase at temperatures of >400°C. The CDS-1 phase was stable up to temperatures close to 900°C, and exhibited greater specific surface areas and micropore volumes than the PLS-1 phase. The TPD of ammonia and pyridine indicated that the CDS-1 phase exhibited weak acid sites, which were mainly of Lewis type.

REFERENCES

Antoni T., Subotic B., Kaucic V. & Thompson R.W. (1999) Study of the influence of the silica source on the properties of silicate solutions and particulate properties of zeolite X. *Studies in Surface Sciences and Catalysis*, **125**, 13–20.

Asakura Y., Osada S., Hosaka N., Terasawa T. & Kuroda K. (2014) Optimal topotactic conversion of layered octosilicate to RWR-type zeolite by separating the formation stages of interlayer condensation and elimination of organic guest molecules. *Dalton Transactions*, **43**, 10392–10395.

Bagnasco G. (1996) Improving the selectivity of NH_3 TPD measurements. *Journal of Catalysis*, **159**, 249–252.

Bhat R.N. & Kumar R. (1990) Synthesis of zeolite beta using silica gel as a source of SiO_2. *Journal of Chemical Technology and Biotechnology*, **48**, 453–466.

Bi Y., Blanchard J., Lambert J.F., Millot Y., Casale S., Zeng S., Nie H. & Li D. (2012) Role of the Al source in the synthesis of aluminum magadiite. *Applied Clay Science*, **57**, 71–78.

Boukadir D., Bettahar N. & Derriche Z. (2002) Synthesis of zeolites 4A and HS from natural materials. *Annales de Chimie - Science des Materiaux*, **27**, 1–13.

Brenner S., McCusker L.B. & Baerlocher Ch. (2002) The application of structure envelopes in structure determination from powder diffraction data. *Journal of Applied Crystallography*, **35**, 243–252.

Burton A.W. (2007) A priori phase prediction of zeolites: Case study of the structure-directing effects in the synthesis of MTT-type zeolites. *Journal of the American Chemical Society*, **129**, 7627–7637.

Burton A.W. & Zones S.I. (2007) Organic molecules in zeolite synthesis: Their preparation and structure-directing effects. *Studies in Surface Science and Catalysis*, **168**, 137–179.

Buzzoni R., Bordiga S., Ricchiardi G., Lamberti C. & Zecchina A. (1996) Interaction of pyridine with acidic (H-ZSM5, H-β, H-MORD zeolites) and superacidic (H-Nafion membrane) systems: An IR investigation. *Langmuir*, **12**, 930–940.

Cañizares P., Durán A., Dorado F. & Carmona M. (2000) The role of sodium montmorillonite on bounded zeolite-type catalysts. *Applied Clay Science*, **16**, 273–287.

Cui M., Wang Y., Liu X., Sun J., Lv N. & Meng C. (2014) Solvothermal conversion of magadiite into zeolite omega in a glycerol-water system. *Journal of Chemical Technology and Biotechnology*, **89**, 419–424.

Cundy C.S. & Cox P.A. (2004) The hydrothermal synthesis of zeolites: history and development from the earliest to the present time. *Chemical Review*, **103**, 663–701.

Cundy C.S. & Cox P.A. (2005) The hydrothermal synthesis of zeolites: precursors, intermediates and reaction mechanism. *Microporous Mesoporous Materials*, **82**, 1–78.

Den Ouden C.J.J., Datema K.P., Vissar F., Mackay M. & Post M.F.M. (1991) On the dynamics of organic-zeolite interactions: tetramethylammonium in sodalite. *Zeolites*, **11**, 418–424.

Dhainaut J., Daou J., Bidal Y., Bats N., Harbuzaru H., Lapisardi A., Chaumeil A., Defoin A., Rouleau L. & Patarinb J. (2013) One-pot structural conversion of magadiite into MFI zeolite nanosheets using mononitrogen surfactants as structure and shape-directing agents. *Crystal Engineering Communications*, **15**, 3009–3015.

https://doi.org/10.1180/claymin.2016.051.5.07 Published online by Cambridge University Press

Dutta P.K., Barco B. & Shieh D.C. (1986) Raman spectroscopic studies of the tetramethylammonium ion in zeolite cages. *Chemistry and Physics Letters*, **127**, 200–204.

Eypert-Blaison C., Humbert B., Michot L.J., Pelletier J. M., Sauzéat E. & Villiéras F. (2001) Structural role of hydration water in Na- and H-magadiite: A spectroscopic study. *Chemistry of Materials*, **13**, 4439–4446.

Fan W., Shirato S., Gao F., Ogura M. & Okubo T. (2006) Phase selection of FAU and LTA zeolites by controlling synthesis parameters. *Micropororous and Mesoporous Materials*, **89**, 227–234.

Gontier S. & Tuel A. (1996) Synthesis of titanium silicalite-1 using amorphous SiO_2 as silicon source. *Zeolites*, **16**, 184–195.

Gregg S.J. & Sing K.S.W. (1982) *Adsorption, Surface Area and Porosity.* Academic Press, London, 154 pp.

Günter E. (2007) Silicon-29 NMR of solid silicates. In: *Encyclopedia of Magnetic Resonance* (R.K. Harris & R. Wasylishen, editors in chief). John Wiley-Blackwell, Oxford, UK.

Hamidi F., Benguedda A., Di Renzo F. & Fajula F. (2003) Control of crystal size and morphology of mordenite. *Catalysis Letters*, **87**, 149–152.

Hamilton K.E., Coker E.N., Sacco Jr. A., Dixon A.G. & Thompson R.W. (1993) The effects of the silica source on the crystallization of zeolite NaX. *Zeolites*, **13**, 645–653.

Hong S.B. (1995) Raman spectra of tetramethylammonium ion-containing molecular sieves. *Microporous Materials*, **4**, 309–317.

Ikeda T., Akiyama Y., Oumi Y., Kawai A. & Mizukami F. (2004) The topotactic conversion of a novel layered silicate into a new framework zeolite. *Angewandte Chemie, International Edition*, **43**, 4892–4896.

Ikeda T., Kayamori S. & Mizukami F. (2009) Synthesis and crystal structure of layered silicate PLS-3 and PLS-4 as a topotactic zeolite precursor. *Journal of Materials Chemistry*, **19**, 5518–5525.

Kalipcilar H. & Culfaz A. (2001) Influence of nature of silica source on template-free synthesis of ZSM-5. *Crystal Research and Technology*, **36**, 1197–1207.

Karami D. & Rohani S. (2009) A novel approach for the synthesis of zeolite Y. *Industrial and Engineering Chemistry Research*, **48**, 4837–4843.

Kawai A., Urabe Y., Itoh T. & Mizukami F. (2010) Immobilization of isysozyme on the layered silicate RUB-15. *Materials Chemistry and Physics*, **122**, 269–272.

Khabtou S., Chevreau T. & Lavalley J.C. (1994) Quantitative infrared study of the distinct acidic hydroxyl groups contained in modified Y zeolites. *Microporous Materials*, **3**, 133–148.

Kim S.J., Kim M.H., Seo G. & Uh Y.S. (2012) Preparation of tantalum-pillared magadiite and its catalytic performance in Beckmann rearrangement. *Research Chemistry and Intermediate*, **38**, 1181–1190.

Kondo J.N., Nishitani R., Yoda E., Yokoi T., Tatsumi T. & Domen K. (2010) A comparative IR characterization of acidic sites on HY zeolite by pyridine and CO probes with silica-alumina and γ-alumina references. *Physical Chemistry Chemical Physics*, **7**, 11576–11586.

Kooli F. & Yan L. (2009) Thermal stable cetyl trimethylammonium-magadiites: influence of the surfactant solution type. *Journal of Physical Chemistry C*, **113**, 1947–1952.

Kooli F., Mizukami F., Kiyozumi Y. & Akiyama Y. (2001a) Hydrothermal conversion of Na-magadiite to a new silicate layered structure in a TMAOH-water-1,4-dioxane system. *Journal of Materials Chemistry*, **11**, 1946–1950.

Kooli F., Kiyozumi Y. & Mizukami F. (2001b) Conversion of protonated magadiite to a crystalline microporous silica phase via a new layered silicate. *ChemPhysChem*, **2**, 549–551.

Kooli F., Kiyozumi Y., Rives V. & Mizukami F. (2002) Synthesis and textural characterization of a new microporous silica material. *Langmuir*, **18**, 4103–4110.

Kooli F., Yan L., Alshahateet S.F., Siril P. & Brown R. (2008) Effect of pillared clays on the hydroisomerization of *n*-heptane. *Catalysis Today*, **131**, 244–249.

Kooli F., Yan L., Hbaieb K. & Al-Faze R. (2016a) Characterization and catalytic properties of porous clay heterostructures from zirconium-intercalated clay and its pillared derivatives. *Microporous and Mesoporous Materials*, **226**, 482–492.

Kooli F., Yan L., Hbaieb K. & Al Faze R. (2016b) A novel synthetic route to obtain RUB-15 phase by pseudo solid-state conversion. *Microporous and Mesoporous Materials*, **228**, 116–122.

Kresnawahjuesa O., Gorte R.J., de Oliveira D. & Lau L.Y. (2002) A simple, inexpensive, and reliable method for measuring Brønsted-acid site densities in solid acids. *Catalysis Letters*, **82**, 155–160.

Lagaly G., Beneke K. & Weiss A. (1975) Magadiite and H-magadiite: II. H-magadiite and its intercalation compounds. *American Mineralogist*, **60**, 650–658.

Lee S.R., Han Y.S., Park M., Park C.S. & Choy J.H. (2003) Nanocrystalline sodalite from Al_2O_3 pillared clay by solid-solid transformationn. *Chemistry of Materials*, **15**, 4841–4845.

Li Q., Mihailova B., Creaser D. & Sterte J. (2000) The nucleation period for crystallization TPA-silicalite-1 with varying silica source. *Microporous and Mesoporous Materials*, **40**, 53–62.

Li Q.H., Mihailova B., Creaser D. & Sterte J. (2001) Aging effects on the nucleation and crystallization kinetics of colloidal TPA-silicalite-1. *Microporous and Mesoporous Materials*, **43**, 51–59.

Li C.P., Huang C.M., Hsieh M.T. & Wei K.H. (2005) Properties of covalently bonded layered-silicate/polystyrene nanocomposites synthesized via atom transfer radical polymerization. *Journal of Polymer Science. Part A. Polymer Chemistry*, **43**, 534–542.

https://doi.org/10.1180/claymin.2016.051.5.07 Published online by Cambridge University Press

Marler B., Wang Y., Song J. & Gies H. (2014) Topotactic condensation of layer silicates with ferrierite-type layers forming porous tectosilicates. *Dalton Transactions*, **43**, 10396–10416.

Moura M.H. & Pastore H.O. (2014) Functionalized mesoporous solids based on magadiite and [Al]-magadiite. *Dalton Transactions*, **43**, 10471–10483.

Niwa M. & Katada N. (2013) New method for the temperature-programmed desorption (TPD) of ammonia experiment for characterization of zeolite acidity: a review. *The Chemical Record*, **13**, 432–455.

Oberhagemann U., Bayat P., Marler B., Gies H. & Rius J. (1996) A layer silicate: Synthesis and structure of the zeolite precursor RUB-15- [$N(CH_3)_4]_8[Si_{24}O_{52}(OH)_4].20H_2O$. *Angewandte Chemie, International edition*, **23–24**, 2869–2872.

Ogawa M., Yamamoto M. & Kuroda K. (2002) Intercalation of an amphiphilic azobenzene derivative into the interlayer space of a layered silicate, magadiite. *Clay Minerals*, **36**, 263–266.

Ouasri A., Rhandour A., Dhamelincourt M.C., Dhamelincourt P. & Mazzah A. (2002) Vibrational study of $(CH_3)4NSbCl_6$ and $[(CH_3)4N]_2SiF_6$. *Spectrochimica Acta A: Molecular and Biomolecular Spectroscopy*, **58**, 2779–2788.

Pál-Borbély G., Beyer H.K., Kiyozumi Y. & Mizukami F. (1997) Recrystallization of magadiite varieties isomorphically substituted with aluminum to MFI and MEL zeolites. *Microporous Materials*, **11**, 45–51.

Park K.W., Jung J.H., Seo H.J. & Kwon O.Y. (2009) Mesoporous silica-pillared kenyaite and magadiite as catalytic support for partial oxidation of methane. *Microporous Mesoporous Materials*, **121**, 219–225.

Pinar A.B., Gómez-Hortigüela L. & Pérez-Pariente J. (2007) Cooperative structure directing role of the cage-forming tetramethylammonium cation and the bulkier benzylmethylpyrrolidinium in the synthesis of zeolite ferrierite. *Chemistry of Materials*, **19**, 5617–5626.

Ríos C.A., Williams C.D. & Fullen M.A. (2009) Nucleation and growth history of zeolite LTA synthesized from kaolinite by two different methods. *Applied Clay Science*, **42**, 446–454.

Ruiz R., Blanco C., Pesquera C., Gonzalez F., Benito I. & Lopez J.L. (1997) Zeolitization of a bentonite and its application to the removal of ammonium ions from waste water. *Applied Clay Science*, **12**, 73–83.

Selvam T., Bandarapu B., Mabande G.T.P.H., Toufar H. & Schwieger W. (2003) Hydrothermal transformation of a layered sodium silicate, kanemite, into zeolite Beta (BEA). *Microporous and Mesoporous Materials*, **64**, 41–50.

Selvam T., Inayat A. & Schwieger W. (2014) Reactivity and applications of layered silicates and layered double hydroxides. *Dalton Transactions.*, **43**, 10365–10387.

Solânea F., Ramos O., de Pietre Mendelssom K. & Pastore H.O. (2013) Lamellar zeolites: an oxymoron? *Royal Society of Chemistry Advances*, **3**, 2084–2111.

Suk-Bong H. (1995) Raman spectra of tetramethylammonium ion-containing molecular sieves. **4**, 309–317.

Wang Y., Shang Y., Wu J., Zhu J., Yang Y. & Meng C. (2010a) Recrystallization of magadiite into offretite in the presence of tetramethylammonium cations. *Journal of Chemical Technology and Biotechnology*, **85**, 279–282.

Wang Y., Wu J., Zhu J., Yang Y., Qi L., Ji S. & Meng C. (2010b) The influence of short-chain tetraalkylammonium cations on the recrystallization of magadiite into zeolites. *Microporous and Mesoporous Materials*, **135**, 143–146.

Warzywoda J., Dixon A.G., Thompson R.W. & Sacco Jr. A. (1995) Synthesis and control of the size of large mordenite crystals using porous silica substrates. *Journal of Materials Chemistry*, **5**, 1019–1025.

Warzywoda J., Dixon A.G., Thompson R.W., Sacco Jr. A. & Suib S.L. (1996) The role of the dissolution of silicic acid powders in aluminosilicate synthesis mixtures in the crystallization of large mordenite crystals. *Zeolites*, **16**, 125–137.

Werner P.E., Eriksson L. & Westdahl M. (1985) TREOR, a semi-exhaustive trial-and-error powder indexing program for all symmetries. *Journal of Applied Crystallography*, **18**, 367–370.

Wiersema G.S. & Thompson R.W. (1996) Nucleation and crystal growth of analcime from clear aluminosilicate solutions. *Journal of Materials Chemistry*, **6**, 1693–1699.

Xue T., Liu H. & Wang Y.M. (2015) Synthesis of hierarchical ferrierite using piperidine and tetramethylammonium hydroxide as cooperative structure-directing agents. *Royal Society of Chemistry Advances*, **5**, 12131–12138.

Yin X., Li Z., Wang S., Chu N., Yang J. & Wang J. (2015) Hydrothermal synthesis of hierarchical zeolite T aggregates using tetramethylammonium hydroxide as a single template. *Microporous and Mesoporous Materials.*, **201**, 247–257.

https://doi.org/10.1180/claymin.2016.051.5.07 Published online by Cambridge University Press